Achromatic metalens array for full-colour light-field imaging

Ren Jie Lin[1,9], Vin-Cent Su[2,9], Shuming Wang[3,4,5,9], Mu Ku Chen[1,9], Tsung Lin Chung[1], Yu Han Chen[1], Hsin Yu Kuo[1], Jia-Wern Chen[1], Ji Chen[3,4,5], Yi-Teng Huang[1], Jung-Hsi Wang[6], Cheng Hung Chu[7], Pin Chieh Wu[7], Tao Li[3,4,5], Zhenlin Wang[3,5], Shining Zhu[3,4,5]* and Din Ping Tsai[1,7,8]*

A light-field camera captures both the intensity and the direction of incoming light[1-5]. This enables a user to refocus pictures and afterwards reconstruct information on the depth of field. Research on light-field imaging can be divided into two components: acquisition and rendering. Microlens arrays have been used for acquisition, but obtaining broadband achromatic images with no spherical aberration remains challenging. Here, we describe a metalens array made of gallium nitride (GaN) nanoantennas[6] that can be used to capture light-field information and demonstrate a full-colour light-field camera devoid of chromatic aberration. The metalens array contains an array of 60×60 metalenses with diameters of 21.65 μm. The camera has a diffraction-limited resolution of 1.95 μm under white light illumination. The depth of every object in the scene can be reconstructed slice by slice from a series of rendered images with different depths of focus. Full-colour, achromatic light-field cameras could find applications in a variety of fields such as robotic vision, self-driving vehicles and virtual and augmented reality.

The concept of the light-field camera was first suggested by Gabriel Lippmann, who introduced integral photography in 1908[1]. Adelson proposed the plenoptic function in 1991[2] and demonstrated the plenoptic camera the following year[3]. In 1996, Levoy and Hanrahan simplified the plenoptic function from seven dimensions to four in a static scene with fixed illumination[4]. Isaksen et al. showed the capability of refocusing a light-field camera array to captured view point images in 2000[7]. During the development of light-field-imaging theory, many imaging devices have been produced, such as the coded aperture camera[8] and the microlens array-based camera[9]. Compared with conventional optical imaging, light-field imaging can not only provide two-dimensional intensity but also enable scene reconstruction with refocused images and depth information[10-12]. The research on light-field imaging can be divided simply into two areas: light-field image acquisition[13-16] and image rendering[17-20]. Microlens arrays have been used for this purpose in light-field cameras; however, it is difficult to obtain broadband achromatic and low-defect microlens arrays without spherical aberrations. Another inherent disadvantage is that the diameter of a single microlens is still too large to achieve a feasible depth of field close to that of the natural compound eyes of insects.

Metalenses[21-24] have successfully demonstrated excellent optical properties for many applications, such as imaging[6], spectroscopy[25] and full-colour routing[26]. The combination of light-field imaging and a multiplexed metalens array composed of sublenses with different functionalities, including differences in the optical axis, focal length and wavelength, was proposed by Brongersma and collaborators[27]. However, chromatic aberration is still an inevitable issue in metalenses for imaging applications. Achromatic metalenses using integrated-resonant units have recently been shown to exhibit excellent aberration-free imaging capability[6,28]. White light images with a spatial resolution of 2.2 μm and full-colour imaging obtained by a 50 μm diameter GaN achromatic metalens have also been reported[6]. The inherent advantages of the achromatic metalens are freedom from spherical aberration, long depth of field, light weight and compact size. In this paper, we implement light-field imaging with a compact and flat GaN achromatic metalens array to capture multidimensional light-field information. Our experiment used a 60×60 array of GaN achromatic metalenses with individual diameters of 21.65 μm. The spatial scene can be reconstructed slice by slice from a series of rendered images with different depths of focus. The depths of every object in the scene are determined, which further demonstrates the feasibility of velocity measurement.

A schematic of focused light-field imaging with an achromatic metalens array is presented in Fig. 1a, which shows how reconstructed images with different depths of focus can be rendered from the subimages captured from the sensing plane. The ability to eliminate the chromatic aberration of our metalens is related to the introduction of phase compensation to metalenses[6]. Solid and inverse GaN nanoantennas with different geometries, which are considered waveguides supporting various higher-order modes, are arranged on a sapphire substrate to achieve the phase compensation requirements. Among the feasible dielectric materials for metalenses reported previously, GaN shows the advantages of having lower fabrication cost and higher efficiency than silicon and TiO_2. A single achromatic metalens consists of over 9,000 GaN nanoantennas. The details of their structural parameters are provided in Supplementary Fig. 1 and Supplementary Table 1. The achromatic metalens array is fabricated by using standard electron-beam lithography and several hard mask transfer and etching processes (see the Fabrication section in the Supplementary Information for details). The corresponding scanning electron microscope (SEM) images are shown in

[1]Department of Physics, National Taiwan University, Taipei, Taiwan. [2]Department of Electrical Engineering, National United University, Miaoli, Taiwan. [3]National Laboratory of Solid State Microstructures, School of Physics, College of Engineering and Applied Sciences, Nanjing University, Nanjing, China. [4]Key Laboratory of Intelligent Optical Sensing and Manipulation, Ministry of Education, Nanjing, China. [5]Collaborative Innovation Center of Advanced Microstructures, Nanjing, China. [6]Department of Electrical Engineering and Graduate Institute of Electronics Engineering, National Taiwan University, Taipei, Taiwan. [7]Research Center for Applied Sciences, Academia Sinica, Taipei, Taiwan. [8]College of Engineering, Chang Gung University, Taoyuan, Taiwan. [9]These authors contributed equally: Ren Jie Lin, Vin-Cent Su, Shuming Wang, Mu Ku Chen. *e-mail: zhusn@nju.edu.cn; dptsai@phys.ntu.edu.tw
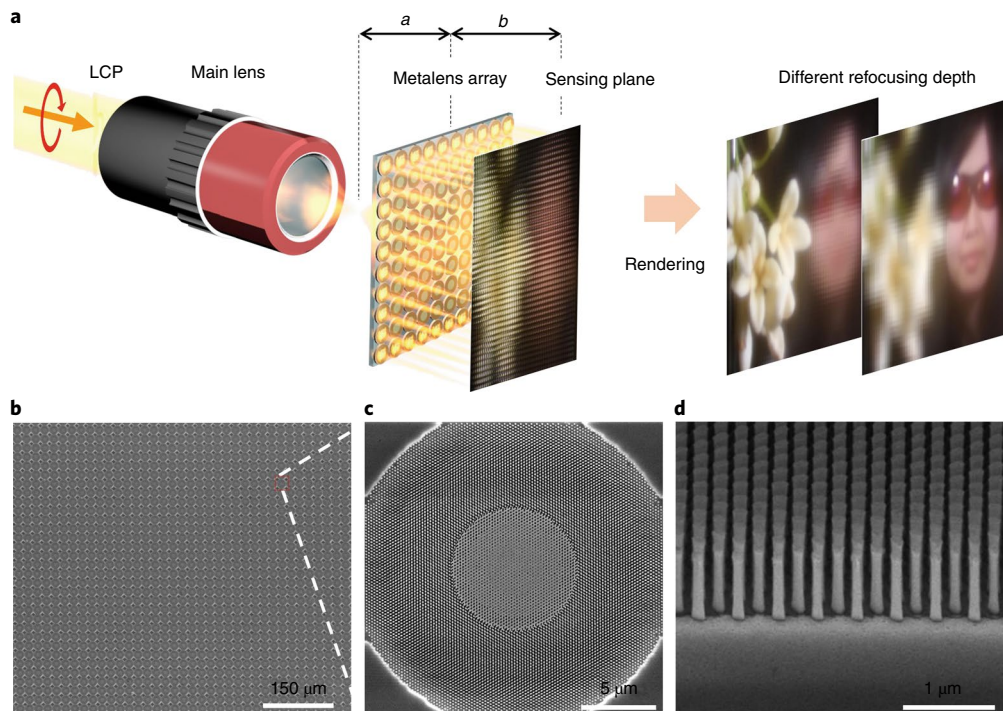
Fig. 1 | Light-field imaging with a metalens array. a, Schematic diagram of light-field imaging with metalens array and rendered images. An objective is used to collect the circularly polarized light on the achromatic metalens array and form an intermediate image in front of the achromatic metalens array. The achromatic metalens array consists of 60×60 individual metalenses with a designed focal length $f = 49\,\mu m$, $d = 21.65\,\mu m$ and numerical aperture 0.2157. LCP, left-handed circular polarization. **b,** SEM image of achromatic metalens array. **c,** Zoomed-in SEM image of a single metalens (red square in **b**) with nanopillars and inverse GaN-based structures. **d,** Tilted-view zoomed-in image of GaN nanopillars.

Fig. 1b–d. The top view of the fabricated metalens array shows well-defined nanopillars and inverse structures, exhibiting great fidelity to our design. More details of the characteristics of the metalens, including the optical images, different viewpoint SEM images, focal length, efficiency and full-width at half-maximum, can be found in Supplementary Figs. 2 and 3. By design, the focal length maintains the same value at different wavelengths from 400 nm to 660 nm, realizing broadband achromatic properties in the visible region. The highest efficiency can be up to 74.8% ± 2.6% at a wavelength of 420 nm, whereas the average efficiency is approximately 39.1% ± 1.8% over the whole working bandwidth. The efficiency is defined as the ratio of the power of the circularly polarized light to that of the incident light with the opposite handedness. The inconsistency in efficiencies for different wavelengths can be attributed to the fluctuation in efficiency in each building block, the numerical aperture of the metalens and the intrinsic loss of GaN[29]. The variation in the efficiency leads to a slight colour cast. However, this cast can be corrected by complementary metal–oxide–semiconductor sensors or the colour balance algorithm after capturing images[6]. To verify the resolving power of our imaging system, the modulation transfer function was also calculated, as shown in Supplementary Fig. 4. The achromatic metalens array forms various subimages with four-dimensional radiance information from each metalens at the sensing plane. The position of the achromatic metalens array for focused light-field imaging follows the Gaussian lens formula:

$$\frac{1}{a} + \frac{1}{b} = \frac{1}{f_{\text{metalens}}} \quad (1)$$

where f_{metalens}, a and b are the focal length of a single metalens, the distance from the main lens image plane to the achromatic metalens array and the distance from the metalens array to the sensing plane, respectively.

Figure 2a shows the focused light-field image captured by a digital single-lens reflex camera with an achromatic metalens array from three objects (letters) in an orderly arrangement with halogen lamp irradiation (purple C, green B and yellow A). The experimental setup used for focused light-field imaging is shown in Supplementary Fig. 5. The distance from the main lens image plane to the metalens array and the distance from the metalens array to the sensing plane are 300 μm and 58.5 μm, respectively, which are determined by the apertures of the metalens, the sensor pixel size and the depth range of the scene. The heights of all objects in this scene are 7.5 mm. Figure 2a consists of 55×40 subimages showing the different perspectives of the scene. An individual subimage comprises 87 pixels. A part of the inverted image of letters in the subimages can be observed in Fig. 2b,c, which shows a portion of Fig. 2a on the boundary between two letters. The quality of every subimage is clear and easy to distinguish. The rendering algorithm for constructing the scene, described in Methods, can arbitrarily render the images with different focusing depths. Figure 2d–f shows the reconstructed images at focusing depths of 48.1 cm, 52.8 cm and 65.3 cm, respectively. The checkerboard effect artefacts (the blurry characteristics of the reconstructed image) found on the other non-focused objects are features of focused light-field imaging.

The scene in Fig. 3 consists of three objects (Earth, a rocket and Saturn made of paper) at different depths. Figure 3a–c shows the rendered images focused on the rocket at depths of 50 cm, 54 cm and 66.5 cm, and Fig. 3d–f shows the corresponding estimated depth maps. The focused light-field-imaging setup is shown in Supplementary Fig. 6. The Earth-to-achromatic metalens array and Saturn-to-achromatic metalens array distances are fixed at 49.5 cm and 67 cm, respectively. The rocket is set as the linear moving target
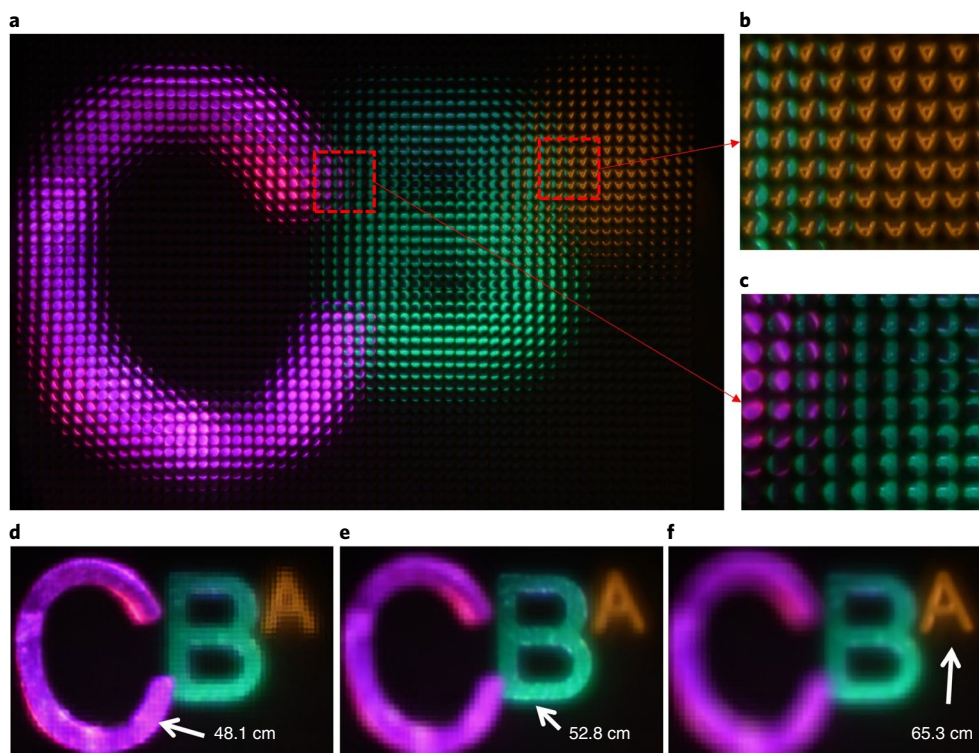
Fig. 2 | Characteristics of the radiance captured by the focused metalens array light-field-imaging system. a, The raw light-field image with the achromatic metalens array. Three letters made from plastic are arranged neatly in the intermediate image space under halogen lamp irradiation (purple C, green B and yellow A). **b,c**, Zoomed-in images of **a. d–f**, Rendered images with focusing depths of 48.1 cm (**d**), 52.8 cm (**e**) and 65.3 cm (**f**).
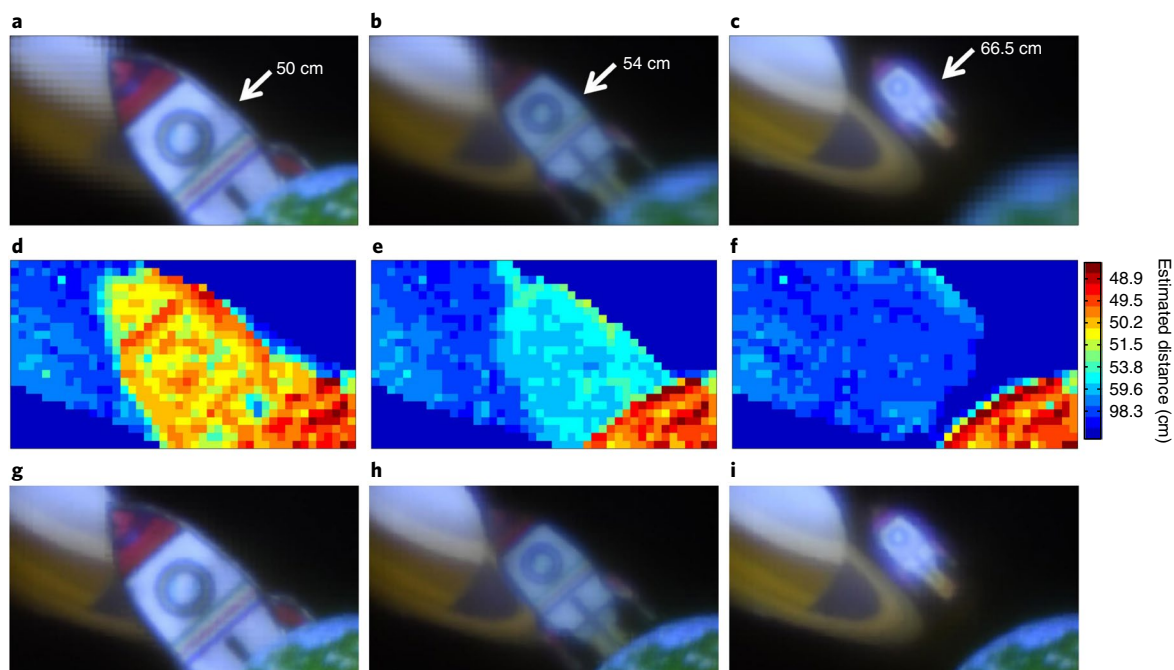
Fig. 3 | Depth estimation of the scene combining Earth, a rocket and Saturn. a–c, Rendered images focusing on the rocket with depths of 50 cm (**a**), 54 cm (**b**) and 66.5 cm (**c**). **d–f**, The estimated depth maps corresponding to images **a–c**. **g–i**, Rendered all-in-focus images with the rocket at different positions between Earth and Saturn.

with constant moving velocity of 1 cm s^{-1}. The depth information can be derived from the disparities between adjacent subimages, and the algorithm for the depth estimation is described in Methods.

As shown in Fig. 3d, when the rocket is next to Earth, the average depth of the rocket (49.8 cm) is close to that of Earth (49.5 cm). When the rocket is moving towards Saturn, its calculated depth also
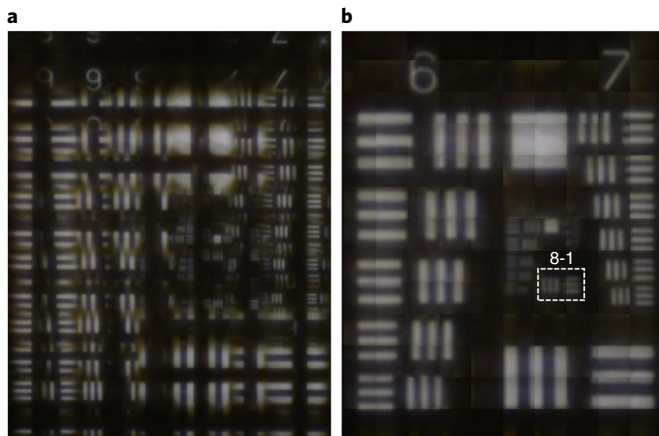
Fig. 4 | Quantification of the imaging resolution of the light-field system with an achromatic metalens array. a, Raw light-field image of the 1951 United States Air Force resolution test chart. **b**, The rendered image of **a**. The white dashed line marks the smallest resolvable target of this system (group 8, element 1).

increases. The results clearly demonstrate that light-field imaging with an achromatic metalens array has the ability to evaluate the depths of multiple objects. A real-time display of the rendering images and depth maps is shown in Supplementary Video 1. More importantly, when the positions of multiple objects can be evaluated, their relative speed can also be detected. Once obtained, the depth information can be used to optimize the patch sizes for different depths and to render the refocused all-in-focus images without artefacts, allowing them to be regarded as an image captured from an infinite depth-of-field system, as shown in Fig. 3g–i.

To assess the imaging resolution limits of the achromatic metalens array, the 1951 United States Air Force resolution test chart, which shows a typical resolvable structure, is used as a target object. The resolution test chart is illuminated by a broadband incoherent light source (a halogen lamp). The optical measurement configuration is shown in Supplementary Fig. 7. Figure 4a shows the light-field image formed by the achromatic metalens array, in which each subimage of a single metalens unit contains the individual information of the target object. The reconstructed image is shown in Fig. 4b after the rendering process. The smallest feature of objects that could be resolved was 1.95 μm in linewidth (group 8, element 1), which was identified by the Rayleigh criterion and indicates the precise fabrication of the achromatic metalens array.

We have shown that the light-field images acquired by an array of 60 × 60 GaN achromatic metalenses with 33,660,000 GaN resonators clearly demonstrate multidimensional optical information, including full-colour imaging and depth. Our work provides additional advantages associated with light-field imaging: elimination of chromatic aberration, polarization selectivity and compatibility of the semiconductor process. Considering its flexibility, the achromatic multiplexed metalens array with integrated functionalities may be promising for multifocusing microscopy, high-dimension quantum technology, hyperspectral microscopy, robotic microvision, unoccupied vehicle sensing, virtual and augmented reality, drones and miniature personal security systems.

Online content

Any methods, additional references, Nature Research reporting summaries, source data, statements of data availability and associated accession codes are available at https://doi.org/10.1038/s41565-018-0347-0.

References

1. Lippmann, G. Epreuves reversibles donnant la sensation du relief. *J. Phys. Theor. Appl.* **7**, 821–825 (1908).
2. Adelson, E. H. & Bergen, J. R. in *Computational Models of Visual Processing* (eds Landy, M. S. & Movshon, J. A.) 3–20 (MIT Press, Cambridge, 1991).
3. Adelson, E. H. & Wang, Y. A. Single lens stereo with a plenoptic camera. *IEEE Trans. Pattern Anal. Mach. Intell.* **14**, 99–106 (1992).
4. Levoy, M. & Hanrahan, P. Light field rendering. In *Proc. 23rd Annual Conference on Computer Graphics and Interactive Techniques* (ed. Fujii, J.) 31–42 (ACM Press, 1996).
5. Wilburn, B. et al. High performance imaging using large camera arrays. *ACM Trans. Graph.* **24**, 765–776 (2018).
6. Wang, S. M. et al. A broadband achromatic metalens in the visible. *Nat. Nanotechnol.* **13**, 227–232 (2018).
7. Isaksen, A., McMillan, L. & Gortler, S. J. Dynamically reparameterized light fields. In *Proc. 27th Annual Conference on Computer Graphics and Interactive Techniques* (eds Brown, J. S. & Akeley, K.) 297–306 (ACM Press, 2000).
8. Levin, A., Fergus, R., Durand, F. & Freeman, W. T. Image and depth from a conventional camera with a coded aperture. *ACM Trans. Graph.* **26**, 70 (2007).
9. Georgiev, T. G. & Lumsdaine, A. Focused plenoptic camera and rendering. *J. Electron. Imaging* **19**, 021106 (2010).
10. Lumsdaine, A. & Georgiev, T. *Full Resolution Lightfield Rendering* (Adobe Systems, 2008).
11. Georgiev, T. & Lumsdaine, A. Reducing plenoptic camera artifacts. *Comput. Graph. Forum* **29**, 1955–1968 (2010).
12. Zeller, N., Quint, F. & Stilla, U. Depth estimation and camera calibration of a focused plenoptic camera for visual odometry. *ISPRS J. Photogramm. Remote Sens.* **118**, 83–100 (2016).
13. Lin, X., Wu, J. M., Zheng, G. A. & Dai, Q. H. Camera array based light field microscopy. *Biomed. Opt. Express* **6**, 3179–3189 (2015).
14. Pegard, N. C. et al. Compressive light-field microscopy for 3D neural activity recording. *Optica* **3**, 517–524 (2016).
15. Hallada, F. D., Franz, A. L. & Hawks, M. R. Fresnel zone plate light field spectral imaging. *Opt. Eng.* **56**, 081811 (2017).
16. Liu, J. D. et al. Light field endoscopy and its parametric description. *Opt. Lett.* **42**, 1804–1807 (2017).
17. Sahin, E., Katkovnik, V. & Gotchev, A. Super-resolution in a defocused plenoptic camera: a wave-optics-based approach. *Opt. Lett.* **41**, 998–1001 (2016).
18. Wu, C. S., Ko, J. & Davis, C. C. Plenoptic mapping for imaging and retrieval of the complex field amplitude of a laser beam. *Opt. Express* **24**, 29853–29872 (2016).
19. Bok, Y., Jeon, H.-G. & Kweon, I. S. Geometric calibration of micro-lens-based light field cameras using line features. *IEEE Trans. Pattern Anal. Mach. Intell.* **39**, 287–300 (2017).
20. Jin, X., Liu, L., Chen, Y. Q. & Dai, Q. H. Point spread function and depth-invariant focal sweep point spread function for plenoptic camera 2.0. *Opt. Express* **25**, 9947–9962 (2017).
21. Zhu, W. M. et al. A flat lens with tunable phase gradient by using random access reconfigurable metamaterial. *Adv. Mater.* **27**, 4739–4743 (2015).
22. Khorasaninejad, M. et al. Metalenses at visible wavelengths: diffraction-limited focusing and subwavelength resolution imaging. *Science* **352**, 1190–1194 (2016).
23. Tseng, M. L. et al. Metalenses: advances and applications. *Adv. Opt. Mater.* **6**, 1800554 (2018).
24. Hsiao, H. H. et al. Integrated resonant unit of metasurfaces for broadband efficiency and phase manipulation. *Adv. Opt. Mater.* **6**, 1800031 (2018).
25. Khorasaninejad, M., Chen, W. T., Oh, J. & Capasso, F. Super-dispersive off-axis meta-lenses for compact high resolution spectroscopy. *Nano Lett.* **16**, 3732–3737 (2016).
26. Chen, B. H. et al. GaN metalens for pixel-level full-color routing at visible light. *Nano Lett.* **17**, 6345–6352 (2017).
27. Lin, D., Brongersma, M. L., Kik, P. G. & Wetzstein, G. Light-field imaging using a gradient metasurface optical element. US patent 15/358,114 (2017).
28. Wang, S. M. et al. Broadband achromatic optical metasurface devices. *Nat. Commun.* **8**, 187 (2017).
29. Goldys, E. M. et al. Analysis of the red optical emission in cubic GaN grown by molecular-beam epitaxy. *Phys. Rev. B* **60**, 5464–5469 (1999).

Author contributions

R.J.L., V.-C.S., S.W. and M.K.C. contributed equally to this work. R.J.L. and S.W. conceived the design, performed the numerical design, optical measurement and data analysis, and developed the algorithm. R.J.L., S.W., M.K.C. and C.H.C. co-wrote the manuscript. V.-C.S. and J.-W.C. performed the sample preparation. M.K.C., Y.-T.H., H.Y.K., T.L.C., Y.H.C. and C.H.C. built the optical system for measurement. J.C. and P.C.W. performed the numerical simulation and data analysis. J.-H.W. provided GaN film and performed the sample preparation. T.L., Z.W. and S.Z. organized the project, designed experiments, analysed the results and prepared the manuscript.

D.P.T. organized the project, designed and developed the numerical design and optical measurement, analysed the results and prepared the manuscript. All authors discussed the results and commented on the manuscript.

Competing interests

The authors declare no competing interests.

Additional information

Supplementary information is available for this paper at https://doi.org/10.1038/s41565-018-0347-0.

Reprints and permissions information is available at www.nature.com/reprints.

Correspondence and requests for materials should be addressed to S.Z. or D.P.T.

Publisher's note: Springer Nature remains neutral with regard to jurisdictional claims in published maps and institutional affiliations.

Methods

Rendering for images with different depths of focus. A graphical depiction of the rendering algorithm of focused light-field imaging is shown in Supplementary Fig. 8. Each metalens captures different perspectives of the scene, containing positional and angular information on the radiance. Therefore, the specific viewpoint of the scene can be reproduced by grouping some specific pixels of each subimage. We integrate square patches in the centre of each subimage to obtain an image with a specific depth of focus. The integration of different sizes of patches produces different depths of focus[10,11]. From the farthest to the closest depth of focus, the number of pixels of patches used ranges from 47×47 to 5×5, depending on the ratio of a to b.

Depth estimation. We select a square patch in the centre subimage with a suitable size, approximately one-quarter of the metalens diameter (see Supplementary Fig. 9 for the depth estimation algorithm). We then compare the radiance between the patch of the centre subimage and those of adjacent subimages, but with shifts $\mathbf{d}$ (in pixels). The radiance difference $D(\mathbf{d})$ is defined as the sum of the difference from the red, green, blue colour values. Finally, we determine the minimum shift value as the disparity between two metalenses. The disparities indicate the depth information, which can be transformed into the actual distance[11,12].

Code availability

The code used for analyses and figures is available from the corresponding author upon reasonable request.

Data availability

The data that support the plots within this paper and other findings of this study are available from the corresponding authors upon reasonable request.